DRAFT VERSION MAY 26, 2026
Typeset using LaTeX **twocolumn** style in AASTeX631

Open Data from LIGO, Virgo, and KAGRA through the Second Part of the Fourth Observing Run

THE LIGO SCIENTIFIC COLLABORATION, THE VIRGO COLLABORATION, AND THE KAGRA COLLABORATION

ABSTRACT

LIGO, Virgo, KAGRA, and GEO form a network of gravitational-wave observatories. Data and analysis results from this network are made publicly available through the Gravitational Wave Open Science Center (GWOSC). This paper describes open data from this network, including the addition of data from the second part of the fourth observing run (O4b) and selected periods from the preceding engineering run (ER16), which were collected from times spanning April 6th, 2024 to January 28th, 2025. The public data set includes calibrated strain time series for each instrument, data from additional channels used for noise subtraction and detector characterization, and new analysis data products in the online GWOSC release associated with version 5.0 of the Gravitational-Wave Transient Catalog.

1. INTRODUCTION

The Laser Interferometer Gravitational-Wave Observatory (LIGO; Aasi et al. 2015), Virgo (Acernese et al. 2015), KAGRA (Akutsu et al. 2021a) and GEO 600 (Lück et al. 2010; Affeldt et al. 2014; Dooley et al. 2016) are observing the gravitational-wave (GW) universe with unprecedented sensitivity (Abac et al. 2026a). Data from these observatories are shared and jointly analyzed as described in a Memorandum of Agreement (LIGO–Virgo–KAGRA 2019), so that the instruments form a global network. The instruments operate in a series of observing runs, with breaks between observing periods for instrument upgrades and detector commissioning (Abbott et al. 2020a; Capote et al. 2025). Following a proprietary period for data characterization and analysis by the LIGO–Virgo–KAGRA Collaboration (LVK), data from each observing run are publicly released via the Gravitational Wave Open Science Center (GWOSC) for use by the entire scientific community.[1] The schedule of data releases for LIGO is maintained in the LIGO Data Management Plan (LIGO Laboratory 2025).

Data from previous observing runs have been released with a history going back more than a decade, starting with data from initial LIGO released in 2014 (Vallisneri et al. 2015). Data from the advanced-detector era are organized into an ongoing series of observing runs, beginning with data from the first observing run (O1) and second observing run (O2; Abbott et al. 2021a), and continuing with data released from the third observing run (O3; Abbott et al. 2023a).

The fourth observing run (O4) is divided into several parts, with the first part (O4a) spanning time from May 24, 2023 to January 16, 2024. The second part (O4b) spanned the time beginning on April 10, 2024 to January 28, 2025. This paper describes the publicly available data from the LVK with an emphasis on the new O4b public data release, which follows the structure of the previous O4a public data release (Abac et al. 2025b). As described in Subsection 2.1, this data release includes new data from both LIGO and Virgo for the second part (O4b).

Public data include time series strain data from the instruments, additional time series channels describing the instrument state, and segment information describing data quality of each instrument. In addition, the cumulative set of events identified by the LVK Collaboration, known as the Gravitational-Wave Transient Catalog (GWTC) is publicly available. The fifth version of the cumulative catalog (GWTC-5.0; Abac et al. 2026a,b,c) includes events from previous observing runs, those identified in O4b data, along with revised analysis results from O4a.

Both O4a and O4b data releases include an electronic version of the catalogs that can be browsed online and queried through a Representational State Transfer Application Programming Interface (REST API). This paper is included in a suite of papers describing GWTC-5.0 (Abac et al. 2026a,b,c) and is best understood in the context of the related papers.

In Section 2 we discuss the primary data products from GW observatories and their periods of data taking. In Section 3 we explain the basics of calibration of interferometer strain data. Section 4 outlines some non-astrophysical noise sources that impact GW data analysis and noise mitigations. In Section 5 we describe the details for the strain data available on GWOSC and alternative services. Section 6 discusses additional instrumental monitoring channels used for noise subtraction and production of data-quality flags that are now also distributed by GWOSC. Finally, the GWOSC Event Portal that provides electronic catalogs of detected GW transients is described in Section 7.

2. DATA SET OVERVIEW

2.1. *Observing Time*

[1] GWOSC Home Page, https://gwosc.org

The instruments operated in a series of observing runs described in Abac et al. (2026a), with the following dates:

- O1: 12 September 2015 0:00 UTC (GPS 1126051217) to 19 January 2016 16:00 UTC (GPS 1137254417)
- O2: 30 November 2016 16:00 UTC (GPS 1164556817) to 25 August 2017 22:00 UTC (GPS 1187733618)
- O3a: 1 April 2019 15:00 UTC (GPS 1238166018) to 1 October 2019 15:00 UTC (GPS 1253977218)
- O3b: 1 November 2019 15:00 UTC (GPS 1256655618) to 27 March 2020 17:00 UTC (GPS 1269363618)
- O4a: 24 May 2023 15:00 UTC (GPS 1368975618) to 16 January 2024 16:00 UTC (GPS 1389456018)
- O4b: 10 April 2024 15:00 UTC (GPS 1396796418) to 28 January 2025 17:00 UTC (GPS 1422118818)

The O4a and O4b data releases also include additional data from engineering runs carried out immediately before these observing runs (see Appendix A and Section 5.3). Some observational data are also available from other times studied in targeted LVK publications, including data from the GEO 600 (Dooley et al. 2016) and KAGRA (Akutsu et al. 2021a) detectors, as described in LIGO–Virgo–KAGRA (2017, 2024). In particular, GEO and KAGRA performed a joint observing run, called O3GK, from the 7 April 2020 8:00 UTC (GPS 1270281618) to 21 April 2020 0:00 UTC (GPS 1271462418; LIGO–Virgo–KAGRA 2022; Abbott et al. 2022).

The observatories do not record astrophysical data at all times. Many types of phenomena can interrupt data taking, including instrument maintenance and detector improvements, seismic activity, power outages, and instrument lock-loss for other reasons. A comparison of the total amount of observing time for each run is shown in Tables 1 and 2, where the engineering runs are not taken into account (for further details on this, see Sections A and 5.3). When only one detector is listed in the tables, the observing time corresponds to periods in which that detector alone was taking data. The amount of calendar time for each observing run is shown at the top of each table section (e.g., O4a spanned 237 calendar days). O3 includes observing time from both O3a and O3b, as well as a commissioning break with no observing time.

During O4a, Virgo was not observing due to commissioning activities. KAGRA and GEO 600 data were less sensitive than the other observatories, and so were not used for most analyses. Therefore, only data from LIGO are included in the O4a data release (Abac et al. 2025c). The total coincident time with both LIGO Hanford Observatory (LHO) and LIGO Livingston Observatory (LLO) observing simultaneously during O4a was 126.5 days. The O4b data release also includes Virgo data, provided from the offline analysis-ready reconstruction using the `V1:Hrec_hoftRepro1A_16384Hz` channel, alongside the LHO and LLO data. The total coincident observing time for the three detectors amounts to 91.1 days in addition to double detectors time (e.g., the period of time for which only LHO and LLO operated was of 21.6 days). The table shows similar statistics for each of O1, O2, and O3, with additional information on past data releases available in Abbott et al. (2021a) and Abbott et al. (2023a).

2.2. *Time-series Data*

The primary data product from a GW observatory is the calibrated strain data, often called $h(t)$. The strain data are recorded as a time series, so that each time sample records one measurement of the fractional difference in lengths of the interferometer arms, $\Delta L/L$. The LIGO, Virgo, and KAGRA observatories typically use a sampling rate of 16 384 Hz, corresponding to a data rate of $\sim$4 TB per year per instrument for the strain data. This is a small fraction of the total data rate of several PB per year, which includes hundreds of thousands of diagnostic channels to monitor the state of the instrument and the local environment.

For current instruments, the strain time series consists primarily of instrumental noise at most times (Abbott et al. 2020b). The noise levels in the instruments fluctuate over time, so that the sensitivities of the instruments vary. One long-used figure of merit for the instrument sensitivity is the binary neutron star (BNS) inspiral range (Finn & Chernoff 1993; Chen et al. 2021), which is briefly summarized in Abac et al. (2026a), and gives an estimate of the distance to which a detector could detect a BNS coalescence with a signal-to-noise ratio (SNR) of 8 after averaging over sky location and orientation. The variability in the BNS inspiral range over the course of O4a and O4b is shown in Figure 1. The plot shows that the LIGO observatories frequently operated near their peak sensitivity of around 160 Mpc in O4a, with a slight improvement in O4b when Virgo joined with a sensitivity slightly above 50 Mpc. However, there are also times when elevated noise levels cause the sensitivity to drop, as well as times when the detectors are not operating at all or operating for periods too short to make a reliable inspiral range estimate, and in this case the inspiral range is set to zero. This variability in instrument sensitivity is an important feature of the strain data, and needs to be properly accounted for in any analysis. Over the course of O1 through O4, the typical BNS inspiral range of the instruments generally improved for each run due to occasional hardware upgrades and commissioning work at the observatories (Tse et al. 2019; Buikema et al. 2020; Brooks et al. 2021; Driggers et al. 2019; Soni et al. 2021, 2024; Jia et al. 2024; Capote et al. 2025). The evolution of this range is described in Abbott et al. (2020a) and Abac et al. (2026a).

In addition to the strain time series, the observatories also record a large number of auxiliary channels to measure the state of each instrument and the local environment (Nguyen et al. 2021; Huxford et al. 2024). These channels record quantities like laser-power levels, temperatures, seismic

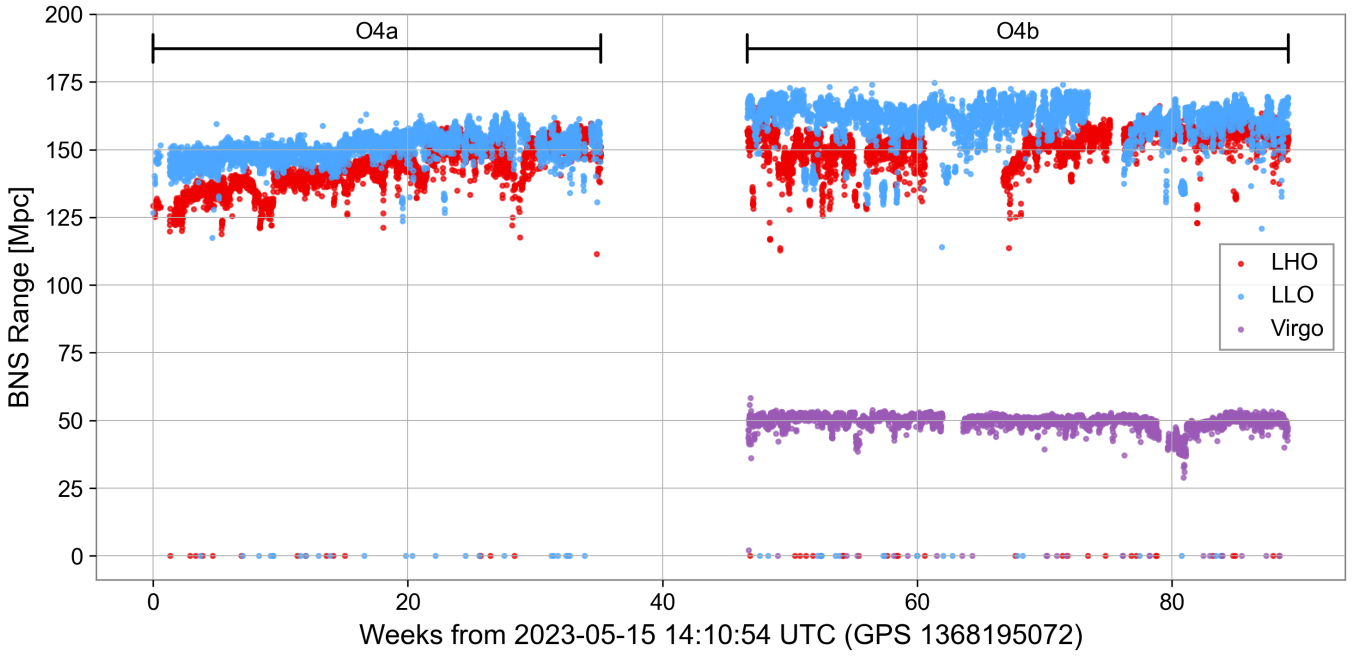

Figure 1. BNS inspiral range over time for O4a and O4b. Each point corresponds to a time interval of 4096 s, corresponding to the time range of one strain data file. If this time range contains a period of data too short to make a reliable inspiral range estimate, the range is set to zero. The fast Fourier transform window length used is 8 s with a 4 s overlap. These inspiral range values are stored as metadata for each strain data file in the GWOSC database and are accessible via the GWOSC website.

motion, angular alignments of mirrors, and many other types of information that can be used to assess instrument performance (Rollins 2016; Soni et al. 2025). A subset of these auxiliary channels is included in the O3, O4a and O4b data releases, and is described in Section 6.

3. CALIBRATION

Ground-based interferometers use feedback control loops to hold the differential arm degree of freedom, $\Delta L(t) = \Delta L_x(t) - \Delta L_y(t)$, in resonance. Calibration refers to the reconstruction of the external differential arm motion $\Delta L(t)$ from the measured differential arm error signal $d_{\rm err}$ using a model of the true interferometer response function R (Abbott et al. 2017; Viets et al. 2018). In the time domain, the differential arm length can be reconstructed through a convolution of the differential arm error signal with the interferometer response function,

$$\Delta L(t) = R(t) \circledast d_{\rm err}(t), \tag{1}$$

where $\circledast$ denotes convolution, implemented using digital finite impulse response filters for the response function (Viets et al. 2018). The strain is defined as the ratio of the differential arm motion to the unperturbed arm length L,

$$h(t) = \frac{\Delta L(t)}{L}, \tag{2}$$

where $L \simeq 3995$ m for LIGO and $L \simeq 3000$ m for Virgo.

3.1. *Calibration Details for LIGO*

Imperfect calibration results in typically small errors in the measured strain. Systematic errors in the imperfect, time-dependent and frequency-dependent calibration model $R^{(\rm model)}$ propagate to the reconstructed LIGO strain data through the ratio $R/R^{(\rm model)}$. For LIGO in O4b, as in O4a, the broadband systematic errors and associated statistical uncertainties in the calibrated strain data are determined on an hourly cadence using a modified version of the methods described in Sun et al. (2020), incorporating additional continuous measurements of the systematic calibration error at discrete frequencies (Wade et al. 2025). The best-estimated systematic errors in the reconstructed strain are left uncorrected in the LIGO strain data, but are reported in these hourly estimates. The overall calibration uncertainties, including both systematic errors and associated statistical uncertainties, for all observing runs are available in the LIGO Document Control Center (LIGO–Virgo–KAGRA 2021a, 2025a).

Calibration methods for past observing runs are described in Abbott et al. (2017); Cahillane et al. (2017); Sun et al. (2020, 2021); Chen et al. (2025) and Acernese et al. (2018, 2022). During O4b, the majority of the final calibrated strain data for both LIGO observatories were computed in near real time (this calibration is designated as C00). An exception was an approximately two-month period from September 3, 2024 19:03:10 UTC to November 14, 2024 19:20:14 UTC, during which the final strain data products were generated offline through a recalibration procedure (C01).

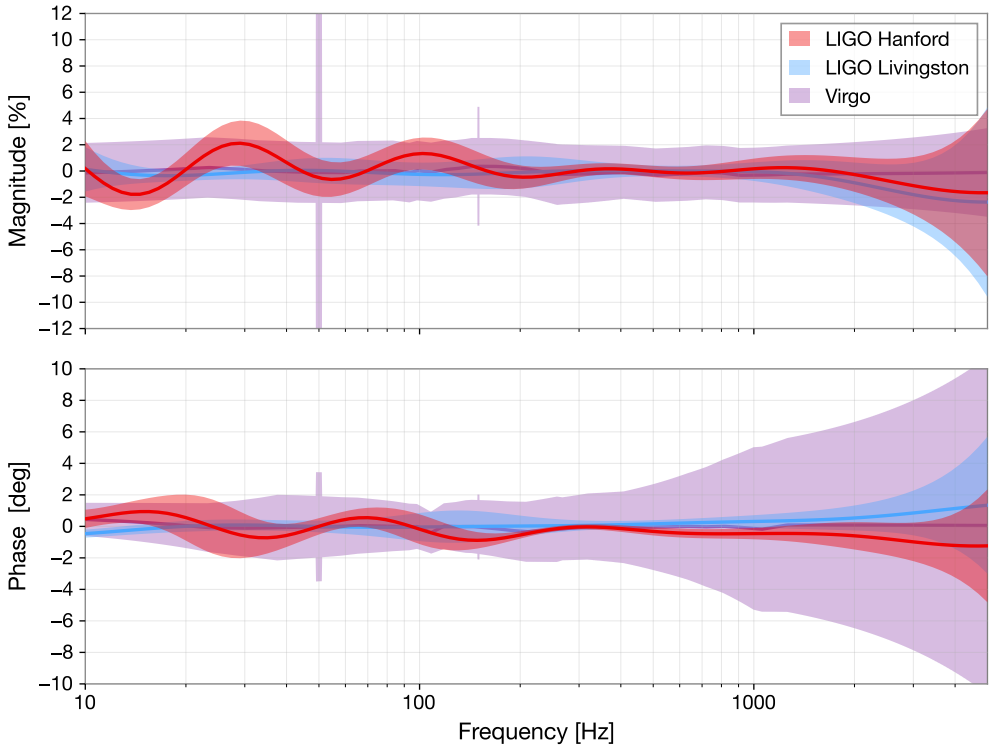

Figure 2. Estimated calibration errors and uncertainties at representative times in O4b (plotted as $R/R^{(\mathrm{model})} - 1$). Frequency-dependent calibration errors for LIGO Hanford (red) and Livingston (blue) are shown for a one-hour period starting at January 27, 2025 12:00:00 UTC. The Virgo frequency-dependent calibration uncertainty is shown for a one-month period starting at September 10, 2024 00:00:00 UTC. The magnitude of the calibration error is shown in the top panel, and the phase (in degrees) in the bottom panel. The solid curves denote the median systematic calibration error (called residual bias in section 3.2), and the shaded regions indicate the associated 1σ uncertainty. These uncertainties are representative of typical calibration performance for LIGO and Virgo during O4b.

An overarching `ANALYSIS_READY` strain data set, denoted `AR01`, was produced to provide a uniform data product for analysis. The `AR01` data set incorporates C01 strain data where available and otherwise uses the corresponding C00 strain data. This differs from O4a, where the `ANALYSIS_READY` data set was denoted `C00_AR`.

The recalibration was performed to address several issues identified in the online calibrated strain data. First, the subtraction of the 60 Hz power mains line and its harmonics (Viets 2019) was not functioning as intended at both LIGO observatories throughout this period; consequently, this subtraction was disabled in the recalibration. Second, at LIGO Hanford, configuration changes to the signal-recycling cavity (SRC) around September 2024, were not fully captured in the online calibration model and are incorporated in the recalibrated data. Finally, a short miscalibration affecting LIGO Hanford on September 25, 2024, lasting approximately two hours, was corrected in the recalibration; this interval includes the time surrounding GW240925_005809, for which astrophysical calibration provided an independent cross-check of the Hanford calibration (Abac et al. 2026).

The photon-calibrator system was used in O4b to inject continuous, sinusoidal excitations at eight frequencies throughout the run (Karki et al. 2016; Bhattacharjee et al. 2024). The systematic error in the calibration at these frequencies was then inferred through the transfer function of the photon-calibrator excitation strain and the reconstructed strain (Wade et al. 2025). The measured systematic error at each of these frequencies was included in the modeled systematic error. Example uncertainty envelopes for the LHO and LLO calibrated strain data toward the end of O4b are shown in Figure 2. The solid curves and shaded regions represent the median systematic calibration error and the associated 1σ uncertainty, respectively, over a one-hour period and are representative of typical calibration conditions during O4b. The calibrated strain data for LIGO in O4b should be considered valid for analyses within the provided hourly uncertainty envelopes in the range 10–5000 Hz.

3.2. *Calibration Details for Virgo*

The Virgo $h(t)$ values are reconstructed by subtracting from the dark-fringe output signal the contribution of each mirror and marionette controls involved in the differential arm length control loop (marionette is an upper part of the mirror suspension system used for alignment controls and low frequency longitudinal controls). The main contributions are the longitudinal controls of the north end, west end and

Table 1. The amount of observing time in days and the corresponding fraction of the total run time for each detector (IFO) combination from O1 to O3. The amount of calendar time for each observing run is shown at the top of each table section.

IFO Combination	Observing Time	Fraction
O1: 129.7 d		
LHO	27.7 d	21.4 %
LLO	16.8 d	13.0 %
LHO, LLO	49.0 d	37.8 %
O2: 268.3 d		
LHO	37.8 d	14.1 %
LLO	33.5 d	12.5 %
Virgo	1.7 d	0.6 %
LHO, LLO	103.0 d	38.4 %
LHO, Virgo	1.7 d	0.6 %
LLO, Virgo	2.2 d	0.8 %
LHO, LLO, Virgo	15.3 d	5.7 %
O3a: 183.0 d		
LHO	5.6 d	3.1 %
LLO	6.3 d	3.4 %
Virgo	15.7 d	8.6 %
LHO, LLO	25.9 d	14.2 %
LHO, Virgo	17.5 d	9.5 %
LLO, Virgo	25.3 d	13.8 %
LHO, LLO, Virgo	80.8 d	44.2 %
O3b: 147.1 d		
LHO	4.5 d	3.1 %
LLO	3.4 d	2.3 %
Virgo	9.3 d	6.3 %
LHO, LLO	22.9 d	15.6 %
LHO, Virgo	14.5 d	9.8 %
LLO, Virgo	13.8 d	9.4 %
LHO, LLO, Virgo	73.4 d	49.9 %
O3: 361.1 d		
LHO	10.1 d	2.8 %
LLO	9.7 d	2.7 %
Virgo	25.0 d	6.9 %
LHO, LLO	48.9 d	13.5 %
LHO, Virgo	31.9 d	8.8 %
LLO, Virgo	39.1 d	10.8 %
LHO, LLO, Virgo	154.3 d	42.7 %
O3GK: 13.7 d		
GEO 600	4.5 d	32.9 %
KAGRA	0.9 d	6.5 %
GEO 600, KAGRA	6.4 d	46.7 %

Table 2. The amount of observing time in days and the corresponding fraction of the total run time for each detector (IFO) combination in O4a and O4b. The amount of calendar time for each observing run is shown at the top of each table section.

IFO Combination	Observing Time	Fraction
O4a: 237.0 d		
LHO	33.3 d	14.1 %
LLO	37.0 d	15.6 %
LHO, LLO	126.5 d	53.4 %
O4b: 293.1 d		
LHO	7.8 d	2.7 %
LLO	22.8 d	7.8 %
Virgo	30.3 d	10.3 %
LHO, LLO	21.6 d	7.4 %
LHO, Virgo	22.1 d	7.5 %
LLO, Virgo	64.2 d	21.9 %
LHO, LLO, Virgo	91.1 d	31.1 %

beam splitter mirrors and, below 100 Hz, the north input and west input marionette controls. Each contribution is obtained using actuator models and optical response models adjusted online via permanent sinusoidal signals injected around 70 Hz and 360 Hz via mirror actuators. The actuator model is defined by the calibration measurements that take the photon calibrator (Grimaud 2025; Estevez et al. 2021a) and Newtonian calibrator (Estevez et al. 2021b; Aubin et al. 2024; Syx 2025) as reference. The resulting $h(t)$ signal is post-processed online with the following steps:

- The bias on $h(t)$ is strongly mitigated by an unbiasing operation done using a bias measurement taken during the previous month. The result is what is called the residual bias. The stability of the bias and residual bias is checked with an online monitoring done with the permanent injected sinusoidal signals (Verkindt et al. 2026; Grimaud et al. 2026).
- All calibration lines injected continuously to monitor the $h(t)$ bias or to get information from the Newtonian calibrator are subtracted.
- A decorrelating linear subtraction, based on the method described in Davis et al. (2019), is used to mitigate any residual broadband noises below 200 Hz coming from the controls of the Michelson and signal recycling cavity degrees of freedom. During O4b, this noise subtraction allowed a gain of about 0.5 Mpc on the BNS inspiral range.

An $h(t)$ offline production has also been done, within the `ANALYSIS_READY` frames production. It includes the

updated state vector (summarized data quality information), the updated $h(t)$ uncertainties and residual bias on a monthly basis and the reprocessing of $h(t)$ whenever needed (the first month of O4b); see Section 5.5 for further details on the ANALYSIS_READY frames. An example of the $h(t)$ uncertainties provided in the ANALYSIS_READY frames is shown in purple in Figure 2. The stability of these frequency-dependent uncertainties over O4b is illustrated by Figure 3.

Details about the calibration procedure, the $h(t)$ online and offline reconstruction and the estimation of $h(t)$ uncertainties and residual bias can be found in Acernese et al. (2026). Details about the Virgo ANALYSIS_READY frames production can be found in Rolland & Verkindt (2025).

4. DATA QUALITY

Noise in the strain data is sometimes approximated as stationary and Gaussian. However, real strain data are also affected by disturbances originating from instrumental and environmental sources (Abbott et al. 2020b; Soni et al. 2025). These artifacts can manifest as broadband, non-Gaussian, short-duration features known as *glitches* (Nuttall 2018; Glanzer et al. 2023), or as narrowband spectral features referred to as *spectral lines* (Covas et al. 2018). In addition, GW observatories can experience periods of degraded performance due to issues in control systems, calibration procedures, or environmental disturbances. These episodes can compromise data quality over extended durations, reducing the sensitivity of the detectors and potentially biasing astrophysical parameter estimation (Pankow et al. 2018; Macas et al. 2022; Kwok et al. 2022; Ghonge et al. 2024; Lecoeuche et al. 2026). To support robust analyses, the LVK employs a suite of data-quality metrics designed to identify and allow mitigation of the impact of instrumental and environmental noise. An overview of LIGO detector characterization efforts is available in Soni et al. (2025). Detector characterization methods for past observing runs are described in Davis et al. (2021); Acernese et al. (2023); Nuttall et al. (2015); Abbott et al. (2016, 2018); Covas et al. (2018); Nguyen et al. (2021); Acernese et al. (2023); and Akutsu et al. (2021b).

Searches for different types of signals exhibit distinct susceptibility to different noise sources, but detector characterization is needed in all cases to remove signals of terrestrial origin and strengthen the confidence of detections. Data-quality products are employed across four broad categories of searches, each with customized detector-characterization methods (Caudill et al. 2021). Compact binary coalescence (CBC) searches (Abac et al. 2026b) target GW signals from the coalescence of neutron stars and/or black holes by applying matched-filtering techniques with modeled waveform templates. GW burst (BURST) analyses (Powell & Lasky 2025) aim to identify short-duration transients without strong assumptions on the signal morphology, e.g., by detecting excess power in the time–frequency representation of the strain data. Continuous wave (CW) searches (Riles 2023) focus on long-duration, nearly monochromatic signals such as GWs emitted by non-axisymmetric rotating neutron stars and various dark matter scenarios. Stochastic (STOCH) searches (Romano & Cornish 2017; Allen 1997) aim to detect a diffuse GW background resulting from the superposition of numerous unresolved sources or early-universe physics.

4.1. *Hardware Injections*

Simulated GW signals, known as *hardware injections* (Biwer et al. 2017), are introduced by physically displacing the interferometer test masses to mimic true astrophysical events and characterize the performance of the detectors and analyses. Hardware injections with signals that mimic expected astrophysical sources are labeled by the simulation type, corresponding to the different classes of potential sources (CBC, BURST, STOCH, or CW). Detector characterization *safety injections* are labeled as DETCHAR injections. These are used to test couplings between channels used to monitor instrumental and environmental noise sources.

We identify auxiliary channels that can be used to indicate a detector problem, for example, when they display excess noise levels. However, some channels are *unsafe* for identifying noise because they respond to astrophysical signals and therefore a response in the auxiliary channel could indicate a real signal. An auxiliary channel is said to be safe to use for identifying noise transients only if it does not respond to astrophysical signals. Safety injections are used to identify unsafe channels. They are performed by actuating the end test-mass mirror using a photon calibrator, thereby generating a response in the primary strain channel (Karki et al. 2016). Channels that exhibit a response to these injections are considered unsafe to use for vetoes, and are identified following the method in Essick et al. (2021).

Hardware injection times are available on the GWOSC website via a tool called Timelines.[2] Additional notes about hardware injections are also provided in the documentation for each data release. In O4b there were no injections labeled CBC, BURST, DETCHAR, or STOCH during observing mode. The only hardware injections present in the released data are CW injections for the LIGO detectors, consisting of simulations of 18 spinning neutron stars whose parameters are provided on the GWOSC website.[3] Their GW frequencies span the range 12–3000 Hz. No GW signal injections were performed for Virgo during O4b, apart from injections used for channel safety testing. Injecting simulated CW signals allows, within the uncertainties of the hardware injection system, a direct end-to-end assessment of degradation in CW signal detection due to imperfect calibration or due to noise subtraction. These injections are almost always present (in O4b, only 5 s of the released LHO data and 6.23% of LLO data do not contain CW injections), but because they are faint and nearly monochromatic, they have minimal impact on transient-signal searches.

[2] Timelines App, https://gwosc.org/timeline/

[3] O4b Injections, https://gwosc.org/O4/o4_inj

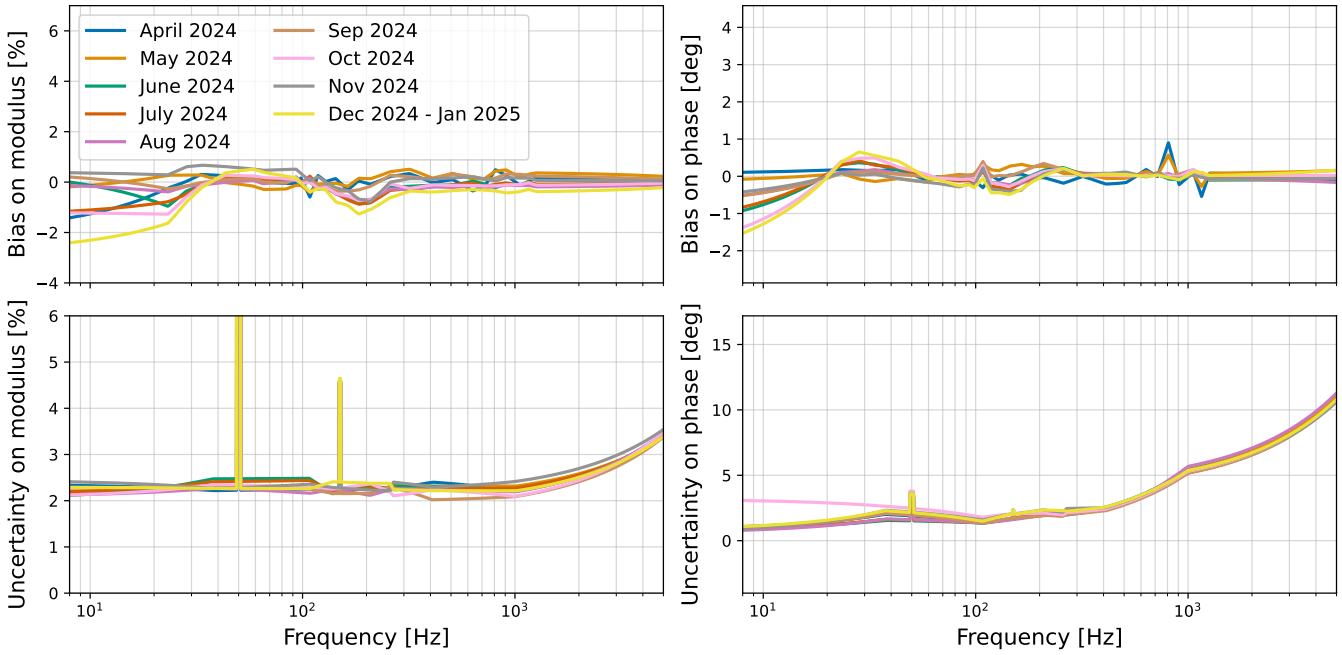

Figure 3. Virgo frequency-dependent calibration uncertainty for each month of O4b. The magnitude and the phase uncertainties are stable from one month to an other.

4.2. *Data-quality Flags*

Data-quality flags are used to identify periods during which the strain data are affected by data-quality issues. These flags are used by analysis pipelines to exclude or down-weight compromised data segments. Flags are classified in order of descending severity, such that the most severe problems are labeled Category 1 (`CAT1`). These flags mark intervals of time affected by well-understood and severe data-quality issues (hardware faults, control-system failures, or known periods of malfunction) during which the strain data are not considered suitable for astrophysical analyses; these times are systematically excluded from all GW searches and parameter-estimation studies. Some searches also apply the less severe Category 2 (`CAT2`), which are typically shorter in duration than `CAT1` (Abac et al. 2026b). Category 3 (`CAT3`) flags are used to identify possible issues of unknown origin which are found through statistical studies. The `CAT2` flags were applied only to BURST searches. The methodology for identifying and applying these flags is described in detail for LIGO in Soni et al. (2025), while Virgo-specific details are provided in Section 4.3.

For CBC analyses, an additional data-quality product used during O4 is the set of statistical flags derived from the `iDQ` supervised-learning framework (Essick et al. 2020). This pipeline evaluates the likelihood that transient noise is present in the strain data based on activity in auxiliary channels that are not expected to be sensitive to astrophysical sources. The `iDQ` pipeline produces several statistical outputs sampled at 128 Hz. The low-latency versions of the `iDQ` outputs are available in the alternate strain release described in Section 5.5; the corresponding channel names are listed in Table 3. The offline `iDQ` outputs are available in LIGO–Virgo–KAGRA (2025b). While the implementation of `iDQ` for the LIGO detectors remained unchanged in O4b relative to O4a, offline `iDQ` outputs were also produced for Virgo data during O4b. The `OK` flag indicates whether the `iDQ` outputs are reliable at a given time, taking the value 1 when valid and 0 otherwise. Other outputs include a normalized `RANK` score that reflects the raw classifier output, an estimated detection efficiency (`EFF`), the false alarm probability (`FAP`) of misclassifying clean times as glitchy, and the log likelihood-ratio (`LOGLIKE`), where positive values suggest the presence of a glitch and negative values suggest clean data. For CBC searches, the `iDQ` flags typically used are derived by thresholding the `LOGLIKE` channel; segments with $\texttt{LOGLIKE} > 5$ are flagged as likely to be glitch-contaminated. Unlike `CAT1` and `CAT2` flags, `iDQ` flags are not applied universally. Search algorithms may choose to use them either as vetoes or to re-rank the significance of candidate events (Abac et al. 2026b).

4.3. *Data Quality Details for Virgo*

For O4b, Virgo provides only `CAT1` data-quality flags. These are based on the automatic `CAT1` flags generated online during data taking, and used by online searches, complemented by a re-evaluation on the `ANALYSIS_READY` data and by additional manual validation (Acernese et al. 2023). The manual checks refined the search for periods of excess noise. Additionally, they targeted anomalous detector behavior or known instrumental issues that may have not been promptly flagged during online operations. The resulting `CAT1` segments define the times

Table 3. The iDQ channel names in the alternate strain release described in Section 5.5, sampled at 128 Hz. *IFO* corresponds to H1 for LHO, L1 for LLO, or V1 for Virgo, and AR stands for ANALYSIS_READY.

	Channel name
OK Flag	*IFO*:IDQ-OK_OVL_10_2048_AR
Rank	*IFO*:IDQ-RANK_OVL_10_2048_AR
False Alarm Prob.	*IFO*:IDQ-FAP_OVL_10_2048_AR
Efficiency	*IfO*:IDQ-EFF_OVL_10_2048_AR
Log likelihood-ratio	*IFO*:IDQ-LOGLIKE_OVL_10_2048_AR

considered unsuitable for scientific analysis in the Virgo open-data release.

Despite a significant improvement in the overall glitch rate with respect to O3, Virgo data during O4b are affected by a known family of recurrent transient noise events, commonly referred to as *25-minute glitches*. These occur approximately every 23–30 min and are characterized by relatively large amplitude, short duration, and a frequency content largely below 200 Hz (Di Renzo 2023). Due to their limited loudness and bandwidth, they are not flagged by the CAT1 procedure. However, their morphology and amplitude make them efficiently handled by the standard data-conditioning steps of transient-search pipelines, including automated data-quality checks and gating procedures, which remove or suppress their impact on searches (Godwin et al. 2020; Chandra et al. 2021; Alléné et al. 2025).

4.4. *Spectral Line Catalog*

Spectral lines are narrowband, often persistent features that appear in the amplitude spectral density of GW strain data. These features arise from a variety of instrumental and environmental sources, including mechanical resonances (e.g., violin-mode resonances from the suspension system), injected lines used for calibration, digital dither signals, and harmonics of the electrical mains. Although their impact on CBC and BURST searches is minimal, spectral lines are a significant concern for persistent searches. Spectral artifacts that overlap with the target signal frequency can severely impact CW searches, which rely on coherence over long timescales. Similarly, STOCH searches are sensitive to lines, especially those of common origin or at harmonics of shared noise sources.

To support the identification and mitigation of these features, the LVK maintains a curated catalog of instrumental spectral lines (Covas et al. 2018; Goetz et al. 2026). The catalog includes both previously known artifacts and newly identified lines, and provides information such as line frequencies, harmonic structure, line widths, detector, temporal occurrence, and, where possible, a suspected source. This information is used by various search pipelines to identify contaminated frequency bins, apply vetoes, or model noise contamination. Spectral line catalogs are publicly available on the GWOSC website as part of the documentation of each run's data release.[4] The complete O4 spectral line list is documented in Goetz et al. (2026).

4.5. *Glitch Subtraction*

Glitches represent a significant source of contamination in strain data, particularly affecting transient searches while having limited impact on persistent searches. In a small number of cases, a glitch occurs in close temporal and spectral proximity to a candidate GW signal, requiring targeted mitigation to reliably recover the astrophysical signal. Subtraction techniques are employed to remove localized excess power in the time–frequency domain (Pankow et al. 2018). One such method is BayesWave (Cornish et al. 2021; Hourihane et al. 2022), which models and subtracts transient noise features from the data without requiring a specific model for the astrophysical signal. A complementary method is linear noise subtraction (Davis et al. 2019), which removes known, repeatable noise contributions using information from auxiliary sensors that monitor the detector environment and instrumental systems.

During O4b, 23 candidate events with a false alarm rate (FAR) below 1 per year required such glitch mitigation in at least one interferometer (Abac et al. 2026c). These events are listed in Table 4, along with their GPS time, affected interferometer(s), and the time–frequency region used to constrain the subtraction and assess residuals. All glitch mitigated data listed in Table 4 were produced with the BayesWave pipeline.

5. STRAIN DATA

Sections 5.1 to 5.4 describe the *default strain-data release*, which can be downloaded directly from the GWOSC website or accessed via the fetch_open_data method of the gwpy package (Macleod et al. 2021).

Alternatively, especially for downloading large data sets, such as an entire observation run, users can download data from the network data server NDS2 (Zweizig et al. 2021) or the Open Science Data Federation (OSDF) service that acts as a storage resource broker and optimizes data access through a worldwide network of data centers.[5] While much of the content in this section is similar across observing runs, Section 5.4 describes differences between runs.

Data in the LVK archives are stored as gravitational-wave frame files (gwf; LIGO–Virgo 2022), a custom binary format developed within the GW community in which data are uniquely identified by a channel name and a frame type. Files for the default strain-data release are created by repackaging the original LVK data, whose identifiers are listed in Table 5 for all observing runs. The best calibration version available is used in the default strain release. In addition to the default strain-data release, several *alternate*

[4] GWOSC data releases, https://gwosc.org/data

[5] Large Scale Data and Computing Resources, https://gwosc.org/osdf

Table 4. List of O4b events from Abac et al. (2026c) with FAR < 1 per year for which glitch subtraction was performed using `BayesWave` (Cornish et al. 2021). For each event, we provide the GPS time, the interferometer (IFO) where subtraction was applied, and the time and frequency windows used for subtraction. The time window indicates the approximate time of the glitch and is referenced from the indicated GPS time, with negative values before the merger and positive values after the merger. A similar table is included in Abac et al. (2026c).

Event	GPS Time	IFO	Time (s)	Frequency (Hz)
GW240514_121713	1399724251.72	LLO	$[0.70, 2.00]$	$[20, 35]$
GW240515_005301	1399769599.11	LLO	$[-4.01, -3.01]$	$[10, 50]$
GW240520_213616	1400276194.97	LLO	$[-0.28, -0.04]$	$[60, 90]$
GW240525_031210	1400641948.64	LLO	$[-4.64, -4.24]$	$[10, 30]$
GW240531_075248	1401177186.46	Virgo	$[-0.30, -0.20]$	$[120, 200]$
GW240601_061200	1401257538.36	LLO	$[0.52, 0.73]$	$[200, 300]$
GW240601_231004	1401318622.03	LLO	$[-5.30, -4.55]$	$[20, 30]$
GW240615_160735	1402502873.33	LLO	$[-0.05, -0.01]$	$[100, 300]$
GW240621_200935	1403035793.53	LLO	$[0.30, 0.40]$	$[200, 300]$
		Virgo	$[-1.80, -1.60]$	$[100, 200]$
GW240629_145256	1403707994.86	LHO	$[-3.10, -2.90]$	$[250, 400]$
GW240705_053215	1404192753.92	Virgo	$[0.90, 1.10]$	$[50, 100]$
GW240902_143306	1409322804.76	Virgo	$[-0.10, 0.10]$	$[300, 400]$
GW240908_082628	1409819206.41	Virgo	$[-0.18, 0.03]$	$[164, 210]$
GW240908_125134	1409835112.27	LLO	$[0.60, 1.20]$	$[20, 30]$
GW240919_061559	1410761777.19	LHO	$[0.20, 0.80]$	$[20, 30]$
GW240920_124024	1410871242.88	LLO	$[0.002, 0.30]$	$[20, 35]$
GW240921_201835	1410985133.79	LLO	$[-4.60, -4.20]$	$[10, 30]$
GW240922_142106	1411050084.39	LHO	$[-0.40, -0.20]$	$[150, 250]$
GW240930_035959	1411704017.96	LLO	$[1.00, 1.80]$	$[10, 800]$
GW241009_220455	1412546713.52	LLO	$[-0.22, 0.58]$	$[10, 30]$
GW241102_144729	1414594067.73	LLO	$[-2.58, -1.63]$	$[10, 30]$
GW241109_033317	1415158416.00	LLO	$[0.60, 1.00]$	$[10, 50]$
GW241125_010116	1416531694.78	LHO	$[-0.60, -0.30]$	$[20, 40]$

strain channels have also been released starting from O3 (see Section 5.5).

The released calibrated strain data of the observing runs are divided into files containing 4096 s of data each. When data are missing or do not meet the necessary quality standards for analysis, strain values are recorded as `NaN`s.

The strain data are available at both the original sampling rate of 16 384 Hz and a reduced rate of 4096 Hz, referred as 16 kHz and 4 kHz in the remainder of this paper. The downsampling process is carried out using the standard decimation method `scipy.signal.decimate`, from the Python library `SciPy` (Virtanen et al. 2020). Before downsampling, an order 8 Chebyshev type I filter (Smith 1999) is used as an anti-aliasing filter.

The maximum resolvable frequency in a given data set is constrained by the Nyquist–Shannon sampling theorem (Nyquist 1924) and corresponds to half of the sampling rate. Due to the roll-off effect of the anti-aliasing filters applied during resampling, the valid frequency range is slightly lower than the Nyquist frequency. Consequently, for data sampled at 4 kHz, frequencies above approximately 1700 Hz are increasingly attenuated by the anti-aliasing filter, which can suppress but not entirely eliminate usable signal content. For data sampled at 16 kHz, however, the limiting factor is given by the calibration which restricts the valid data to 5 kHz, as described in Section 3.

These considerations on the maximum frequency are a crucial factor to consider when selecting a data set to download. On the other hand, data sampled at higher rates require increased storage space and longer download times. Users should, therefore, select the data set that best aligns with their specific requirements.

5.1. *Structure of the Default Strain-Data Files*

The default strain files include not only the strain data but also information on data quality and injections. The main file formats used for the GWOSC open data are the Hierarchical Data Format (`hdf`; Koziol & Robinson 2018), a data format designed for storing and organizing large data sets that is easily readable by many programming languages, and the

Table 5. Channel names and frame types that allow tracing the provenance of strain data released on GWOSC. H1, L1, V1, G1 and K1 are short versions of the interferometer names. The attribute `CLEAN` in H1 and L1 indicates that noise subtraction (Vajente et al. 2020; Davis et al. 2019; Viets & Wade 2021) was used. `AR` stands for `ANALYSIS_READY`, and indicates that these channels contain only data for times ready to be analysed. The other parts of the names refer in general to the calibration version.

Run	IFO	Channel name	Frame type
O1	LHO	`H1:DCS-CALIB_STRAIN_C02`	`H1_HOFT_C02`
O1	LLO	`L1:DCS-CALIB_STRAIN_C02`	`L1_HOFT_C02`
O2	LHO	`H1:DCH-CLEAN_STRAIN_C02`	`H1_CLEANED_HOFT_C02`
O2	LLO	`L1:DCH-CLEAN_STRAIN_C02`	`L1_CLEANED_HOFT_C02`
O2	Virgo	`V1:Hrec_hoft_V1O2Repro2A_16384Hz`	`V1O2Repro2A`
O3a	LHO	`H1:DCS-CALIB_STRAIN_CLEAN_SUB60HZ_C01`	`H1_HOFT_CLEAN_SUB60HZ_C01`
O3a	LLO	`L1:DCS-CALIB_STRAIN_CLEAN_SUB60HZ_C01`	`L1_HOFT_CLEAN_SUB60HZ_C01`
O3a	Virgo	`V1:Hrec_hoft_16384Hz`	`V1Online`
O3a(last two weeks)	Virgo	`V1:Hrec_hoft_V1O3ARepro1A_16384Hz`	`V1O3Repro1A`
O3b	LHO	`H1:DCS-CALIB_STRAIN_CLEAN_SUB60HZ_C01`	`H1_HOFT_CLEAN_SUB60HZ_C01`
O3b	LLO	`L1:DCS-CALIB_STRAIN_CLEAN_SUB60HZ_C01`	`L1_HOFT_CLEAN_SUB60HZ_C01`
O3b	Virgo	`V1:Hrec_hoft_16384Hz`	`V1Online`
O3GK	GEO 600	`G1:DER_DATA_HD_CLEAN`	`G1_RDS_C02_L3`
O3GK	KAGRA	`K1:DAC-STRAIN_C20`	`K1_HOFT_C20`
O4a	LHO	`H1:GDS-CALIB_STRAIN_CLEAN_AR`	`H1_HOFT_C00_AR`
O4a	LLO	`L1:GDS-CALIB_STRAIN_CLEAN_AR`	`L1_HOFT_C00_AR`
O4b	LHO	`H1:DCS-CALIB_STRAIN_CLEAN_AR01`	`H1_HOFT_AR01`
O4b	LLO	`L1:DCS-CALIB_STRAIN_CLEAN_AR01`	`L1_HOFT_AR01`
O4b	Virgo	`V1:Hrec_hoftRepro1AR_16384Hz`	`HoftAR1U02`

`gwf` format, which is the file format used in the LVK archives as already mentioned.

For all available file formats, file names in the default strain release contain the following information:

- *Obs*: the observatory, i.e. the site, that is indicated by one letter and can have values L for LIGO Livingston, H for LIGO Hanford, V for Virgo, G for GEO 600 or K for KAGRA.
- *IFO*: the interferometer label, created by adding a number to the letter that indicates the observatory. This choice allows the identification of multiple detectors installed in the same site, as was the case for Initial LIGO (Abbott et al. 2009). For the LVK observation runs it can have values H1, L1, V1, G1 or K1.
- *Run*: the observing run name, e.g., O4b.
- *s*`KHZ` or *s*: the sampling rate in kHz, *s* can have values 4 or 16 (4096 Hz or 16 384 Hz).
- `R`*n* or `V`*n*: release number or version number of the file. The letter `V` was used only for O1, then it was avoided because it could be confused with the Virgo interferometer name.
- *GPSstart*: the starting time of the data contained in the file, as a 10-digit GPS value (in seconds).
- *Dur*: the duration in seconds of the file, typically 4096 s.
- *Ext*: the extension corresponding to the file format (`gwf`, `hdf` or `txt`).

The structure of the file names is:

Obs—FrameType—GPSstart—Dur.Ext

where the *FrameType* is *IFO*`_GWOSC_`*Run*_*s*`KHZ_R`*n*.

The `hdf` files contain three folders (or groups).

- The folder *meta* hosts the metadata of the file: *Description*, *DescriptionURL*, *Detector* (e.g., L1), *Observatory* (e.g., L), *Duration*, *GPSstart*, *UTCstart* (duration and starting time, using GPS and UTC standards, respectively, of the segment of data contained in a file), *StrainChannel* and *FrameType* used in the LVK archives as listed in Table 5.
- The folder *strain* contains the array *Strain* of $h(t)$ values with useful attributes such as *Xstart* and *Xspacing* that define the GPS start time of the data contained in the array and the temporal distance between points in the array.
- The folder *quality* contains two subfolders: one for data quality and another for injections. Each subfolder

includes a bitmask that indicates, for each second, the status of data quality or injections, along with a description of each bit in the mask (see Section 5.2 for details).

The GWOSC `gwf` files include three channels (for strain data, data quality, and injections), whose names are listed in Table 6.

Table 6. Channel names in the GWOSC `gwf` files. The nomenclature is similar to that described for the file name conventions: *IFO* is the interferometer, s is the sampling rate, n is the version or release (until now only 1 has been used).

	Channel name
Strain	*IFO*:GWOSC-sKHZ_Rn_STRAIN
Data-quality mask	*IFO*:GWOSC-sKHZ_Rn_DQMASK
Injections mask	*IFO*:GWOSC-sKHZ_Rn_INJMASK

Earlier releases used slightly different conventions described in Section 5.4.

5.2. *Data Quality and Injections in GWOSC Files*

The data-quality information is encoded in the default strain release as a bitmask following the structure described in Table 7, with a 1 Hz sampling rate.[6] The meaning of the data-quality flags is explained in Section 4. For template-based binary coalescence searches and minimally modeled searches, labeled respectively as CBC and BURST in Table 7, the bitmask allows 3 categories of data quality (labeled with `CAT1`, `CAT2` and `CAT3`). We keep this structure even for runs in which not all the categories have been used. This choice avoids confusion that could arise if the same bit would have different meaning in different runs. A bit value of 1 indicates the data has passed both the indicated level and lower-level checks; for example, a 1 in the `CBC_CAT2` bit indicates the data pass both `CBC_CAT1` and `CBC_CAT2`.

The data-quality bit labeled as `DATA` is obtained requiring that both `CBC_CAT1` and `BURST_CAT1` are satisfied. This is the criterion that defines what data are released in the *default strain-data release*.

Starting from O4a, two additional bits were added to accommodate Category 1 data quality for STOCH searches (`STOCH_CAT1`) and for CW searches (`CW_CAT1`). Moreover, the Categories 2 and 3 have not been used for the CBC data-quality flag so the corresponding segments coincide with those marked as `CBC_CAT1` (and also `DATA` in this case). BURST searches from O4a did not apply any Category 3 flags. The CW data-quality flag `CW_CAT1` is identical to `CBC_CAT1`.

Table 7. Meaning of the bits in the data-quality bitmask of the GWOSC files. Each bit has value 1 if the data quality passes the corresponding data quality requirement, otherwise the value is zero. Bits 7 and 8 were introduced in O4 and are not present in previous runs (Abbott et al. 2021a, 2023a).

Bit	Short name	Description
0	`DATA`	Data present
1	`CBC_CAT1`	Pass `CAT1` test for CBC search
2	`CBC_CAT2`	Pass `CAT1` and `CAT2` test for CBC search
3	`CBC_CAT3`	Pass `CAT1` and `CAT2` and `CAT3` test for CBC search
4	`BURST_CAT1`	Pass `CAT1` test for BURST search
5	`BURST_CAT2`	Pass `CAT1` and `CAT2` test for BURST search
6	`BURST_CAT3`	Pass `CAT1` and `CAT2` and `CAT3` test for BURST search
7	`STOCH_CAT1`	Pass `CAT1` test for STOCH search
8	`CW_CAT1`	Pass `CAT1` test for CW search

As discussed in Section 4, a crucial way to test the response of the detector is the use of *hardware injections*. In GWOSC files the information about injections is provided as 1 Hz time series containing a bitmask detailed in Table 8.[7] Five bits are used to distinguish injections relevant for astrophysical searches or detector-characterization studies.

Table 8. Meaning of the bits in the injections bitmask of the GWOSC files. The mask indicates when injections are not present, so the bit value is set to 1 to indicate no injection and 0 when there is an injection. `HW_INJ` stands for hardware injection.

Bit	Short name	Description
0	`NO_CBC_HW_INJ`	No CBC injections
1	`NO_BURST_HW_INJ`	No BURST injections
2	`NO_DETCHAR_HW_INJ`	No DETCHAR injections
3	`NO_CW_HW_INJ`	No CW injections
4	`NO_STOCH_HW_INJ`	No STOCH injections

5.3. *Additional Segments in the O4b Strain-Data Release*

As O4a (see Appendix A), also the O4b data release includes data from the engineering run just prior to the start of the run that were used in the search for GW emitted from

[6] See tutorial 3 of https://github.com/gwosc-tutorial/introduction_gwosc_data to learn how to get data-quality information from GWOSC files.

[7] See tutorials in https://gwosc.org/tutorials/ to learn how to get hardware-injection information from GWOSC files.

a supernova, in this case the supernova SN 2024ggi (Ertini et al. 2025). For this reason, the starting time of the data release is 6 April 2024 at 05:37:12 UTC (GPS 1396417050). In addition, for the analysis of GW240925_005809, 10 s of LHO data between 25 September 2024 at 00:57:39 UTC (GPS 1411261077) and 25 September 2024 at 00:57:49 UTC (GPS 1411261087), initially labeled as out-of-observing mode, were, after further investigations, promoted as analysis ready (Abac et al. 2026).

In this way, the amount of time added to the nominal O4b observing run is of 2.9 d for LHO, 3.1 d for LLO and 2.3 d for Virgo and the total observing time for each of the three detectors is 145.5 d, 202.8 d and 210 d, respectively. Using these numbers as reference, we can calculate the percentage of observing time for which data quality fail the categories described in Table 7 and the result is in Table 9.

Table 9. Percentage of the observing time in O4b for which data quality fail the categories described in Table 7. For this calculation, the total amount of observing time is used as reference, including the engineering run just prior to the start of O4b, as discussed in the text.

Short name	LHO	LLO	Virgo
DATA	0.7584%	0.7889%	0.1274%
CBC_CAT1	0.7584%	0.7889%	0.1274%
CBC_CAT2	0.7584%	0.7889%	0.1274%
CBC_CAT3	0.7584%	0.7889%	0.1274%
BURST_CAT1	0.7584%	0.7889%	0.1274%
BURST_CAT2	0.8755%	0.8363%	0.1274%
BURST_CAT3	0.8755%	0.8363%	0.1274%
STOCH_CAT1	0.7584%	0.7889%	0.1274%
CW_CAT1	0.8105%	0.7889%	0.1274%

5.4. *Data Releases from Previous Runs*

The structure described here for the default strain data is largely valid for all data released to date (Abbott et al. 2021a, 2023a; Abac et al. 2025b), with few differences. These concern details in the naming conventions of the files and the channels within them. For example, the *FrameType* mentioned in Section 5.1 is *IFO*_LOSC_*s*_V*n* in O1, the *StrainChannel* and *FrameType* have been present in files since O2, while the channel names in the `gwf` files used only in O1 are shown in Table 10.

The main difference that the user will notice is that up to O3, for each published GW detection, data snippets centered on the event detection time are also released via the GWOSC Event Portal, described in Section 7. These data snippets are provided as plain-text files in addition to the `hdf` and `gwf` files described above. The text files contain strain values in a single column. As of O4, data snippets for most events are no longer published, but instead the associated files from the default strain-data release are linked for each event in the Event Portal, if available at the time of posting the event.

Table 10. Channel names in the GWOSC `gwf` files, used only in O1 for the 4 kHz release (*IFO* is the interferometer name).

	Channel name
Strain	*IFO*:LOSC-STRAIN
Data-quality mask	*IFO*:LOSC-DQMASK
Injections mask	*IFO*:LOSC-INJMASK

5.5. *Alternate Strain Release*

The default strain files described in Sections 5.1–5.4 are prepared after each observing run in order to provide a user-friendly file format that includes the preferred strain channel and the final data quality and injection segments. For O3 and O4, in addition to these user-friendly files, the LVK Collaboration also releases several versions of the strain channel that more closely matches the data available to LVK members before the public data release. These data sets are called alternate strain releases and the frames contained in them are called ANALYSIS_READY frames. Detailed documentation is available on the GWOSC website (LIGO–Virgo–KAGRA 2021b,c, 2025c, 2026).

Starting in O3, alternate strain releases are available for all times the detectors passed the conditions for ANALYSIS_READY, meaning that the detectors were nominally in a good working state. This set of times includes a small amount of time that fails CAT1 data quality, and so there are some times in the alternate strain releases that are not available in the default strain files. Files and strain channels are marked with the tag AR, to indicate that only ANALYSIS_READY times are included.

For O3, those data sets were prepared after the run had ended, with three channels of varying noise subtraction levels for LIGO, and two channels for Virgo: a main and a short-duration one covering a period when additional noise subtraction was needed. See Abbott et al. (2023a) for details about those data sets.

Starting in O4a, the ANALYSIS_READY frames are produced during the run, with three channels of varying noise subtraction levels for LIGO. See Abac et al. (2025b) for details about those data sets. For O4b, analysis ready frames have been produced both for LIGO and Virgo.

For LIGO the process is the following. The calibration pipeline described in Section 3 runs at all times and writes out strain data in 1 s long frame files in order to produce low-latency strain data, including the preferred channel GDS-CALIB_STRAIN_CLEAN. Low-latency analyses, including pipelines that produce public transient

alerts, use these low-latency frame files.[8] To produce the ANALYSIS_READY frames, a frame aggregator collects the 1 s files into ANALYSIS_READY frame files of up to 4096 s long, excludes any times that are not marked as ready for analysis, and adds the tag AR to the channel names. The ANALYSIS_READY frame files are then used for most offline LVK analyses, so that the released product exactly matches data used inside the collaboration. Those ANALYSIS_READY frames are called C00_AR01.

As explained in Section 3, another version of the ANALYSIS_READY frames was produced by incorporating the recalibrated data C01. Those ANALYSIS_READY frames are called AR01.

The O4b alternate strain data sets include several versions of the strain channel for each LIGO instrument, which are summarized in Table 11 and described below. In addition to the strain channels, the O4b ANALYSIS_READY frames also include a number of auxiliary channels that record data-quality information and calibration parameters. The O4b strain channels are (*IFO* corresponds to H1 for Hanford or L1 for Livingston and *frm* means either AR or AR01):

- *IFO*:GDS-CALIB_STRAIN_*frm* This is the calibrated strain data with no noise subtraction applied.
- *IFO*:GDS-CALIB_STRAIN_NOLINES_*frm* This is the calibrated strain data after removing narrowband noise. This channel removes the calibration lines, 60 Hz power-mains line, and harmonics of the power-mains line as described in Viets & Wade (2021).
- *IFO*:GDS-CALIB_STRAIN_CLEAN_*frm* This is the calibrated strain data, after subtracting both narrowband and broadband noise. This applies additional broadband noise subtraction on to the *IFO*:GDS-CALIB_STRAIN_NOLINES_*frm* channel, using the method described in Vajente et al. (2020). This is the recommended channel for transient searches, and it corresponds to the channel name DCS-CALIB_STRAIN_CLEAN_SUB60HZ_C01_AR in O3 (Abbott et al. 2023a).
- *IFO*:GDS-GATED_STRAIN_AR This is the *IFO*:GDS-CALIB_STRAIN_NOLINES_AR channel where times with loud glitches are replaced with zeros by applying a window function around short segments of elevated noise (Zweizig & Riles 2020; Usman et al. 2016). This channel was not used for analyses by the LVK and is not present in AR01 frames. An improved version of the algorithm, as used for several O4 CW searches, is described in Davis et al. (2024).

Virgo ANALYSIS_READY frames were produced in chunks of about one month. The content of the ANALYSIS_READY frames was only C00 $h(t)$ (produced online) or C01 $h(t)$ for the first month of O4b where an offline reprocessing was needed. Whatever its origin (C00 or C01), the name of the Virgo strain channel is V1:Hrec_hoftRepro1AR_16384Hz.

The same ANALYSIS_READY frames also contain the state vector which provides the status of the Virgo interferometer. The name of this channel is V1:DQ_ANALYSIS_STATE_VECTOR and its value is 4095 when the data quality is optimal (interferometer is in science mode, $h(t)$ reconstruction is correct and CAT1 data-quality flag is not activated). By definition of the ANALYSIS_READY frames, $h(t)$ is zero each time the state vector value is not 4095.

Finally, the Virgo ANALYSIS_READY frames contain six other auxiliary channels present only in the frames whose GPS times are a multiple of 1000. Those channels provide the frequency-dependent residual bias modulus and phase and the frequency-dependent uncertainties on $h(t)$ modulus and phase. The prefix of the name of those channels is V1:Hrec_hoftRepro1AR_U02 and the rest of the channel name is used to specify whether the channel refers to the modulus or the phase (see also Rolland & Verkindt (2025)). Details about uncertainty in the calibration for LIGO are provided in separate files as documented in the GWOSC website.[9]

The alternate strain releases are not currently available for direct download from the GWOSC website; instead, they are available via OSDF and NDS2, as discussed earlier in Section 5.

6. AUXILIARY CHANNELS

In addition to the strain time series, LIGO records around 200 000 *auxiliary channels* for each instrument. Auxiliary channels are stored as time series data and record the state of the instrument, the local environment, and a number of digital-filter settings. Auxiliary channels include readings from seismometers, accelerometers, photodiodes, magnetometers, wind monitors, and microphones (Nguyen et al. 2021; Huxford et al. 2024).

The O3, O4a and O4b data releases include the set of LIGO auxiliary channels used for noise subtraction and to produce data-quality flags. These are the ways that auxiliary channels directly contribute to the GWTC-4.0 and GWTC-5.0 analyses. For O3, the auxiliary data release includes about 40 channels for each LIGO detector, corresponding to roughly 80 channels in total. For the O4a and O4b runs, the release includes 25 channels total across both interferometers. The online documentation includes the name of each available channel along with

[8] LIGO/Virgo/KAGRA Public Alerts User Guide, https://emfollow.docs.ligo.org/userguide/

[9] O4 Data Set Technical Details, https://gwosc.org/O4/o4_details/

Table 11. Alternate strain channels in the O4b release and the layers of noise subtraction applied to them. `NOLINES` means that narrowband noise features have been subtracted, while `CLEAN` means that broadband noise features have also been subtracted and `GATED` means the removal of loud glitches. For the first two sets of channels, *IFO* can be H1 or L1.

Frame	Channel name	Narrowband noise subtraction	Broadband noise subtraction	Glitch removal
C00_AR	*IFO*:GDS-CALIB_STRAIN_AR			
	IFO:GDS-CALIB_STRAIN_NOLINES_AR	✓		
	IFO:GDS-CALIB_STRAIN_CLEAN_AR	✓	✓	
	IFO:GDS-GATED_STRAIN_AR	✓		✓
AR01	*IFO*:DCS-CALIB_STRAIN_AR01			
	IFO:DCS-CALIB_STRAIN_NOLINES_AR01	✓		
	IFO:DCS-CALIB_STRAIN_CLEAN_AR01	✓	✓	
AR1U02	V1:Hrec_hoftRepro1AR_16384Hz	✓	✓	

the associated sampling rate and a short description of the channel content.[10]

Auxiliary channels should be used with caution, as the data are not necessarily calibrated and may include times when the data values are missing or corrupt. For example, sensors sometimes break or become disconnected leading to periods of corrupted data. Auxiliary data are available at all times when the detector is in `ANALYSIS_READY` with the exact times marked in segment lists that are available with the data release documentation.

In addition to channels used for noise subtraction and data-quality flags, some auxiliary data have been released on request and are now available on the GWOSC website. For O3, these releases include a data set to support a study of machine learning applied to detector characterization (Gurav et al. 2024) and a study of noise-subtraction methods (Zackay et al. 2023).

Auxiliary-channel data cannot currently be downloaded directly through the GWOSC website or the API. Instead, auxiliary-channel data are available through the NDS2 and OSDF interfaces described in Section 5.

7. EVENT PORTAL

The GWOSC Event Portal provides an online interface to a database of published GW transient events.[11] These events are short-duration GW signals identified in the strain data by searches. They are typically attributed to a signal consistent with a CBC source. Not all events in the Event Portal will be from CBCs, some may be noise with an instrumental origin.

Users of the GWOSC will find an array of data products associated with most events available in the Event Portal, including strain data, segment lists, detection confidence, astrophysical source parameters, and documentation. In most cases, the database also includes links to additional analysis products, such as posterior samples describing source properties and source localizations.

The Event Portal may be accessed as browsable `HTML` webpages or via a REST API. A Python client, named `gwosc`, can be used to query the API and download content.[12] Documentation of the Event Portal and REST API are available on the GWOSC website.

7.1. *User Interfaces to the Data*

GWTC catalogs are a cumulative collection of events. In the Event Portal, *releases* represent sets of new events published in specified LVK publications, such as the new CBC candidates added for GWTC-5.0 (Abac et al. 2026a,b,c), or a collection of events that are related in some other way, such as all the GW transients published in stand-alone discovery papers such as those from O3. As a consequence there are a number of ways to interact with the event data using the Event Portal.

The *Release List View* in the Event Portal displays a list of all available releases, summarized in Table 12. Several releases are labeled marginal, i.e., `GWTC-1-marginal`, `GWTC-2.1-marginal`, `GWTC-3-marginal`, `O3_IMBH_marginal`, which include candidate triggers that have a low significance more consistent with instrumental background than a true GW event.

In addition, there is one release, `GWTC-2.1-auxiliary`, in which revised analyses in `GWTC-2.1` (Abbott et al. 2024) resulted in the demotion of events that were previously identified in `GWTC-2` (Abbott et al. 2021b) as statistically significant. These are included separately for completeness.

Prior to `GWTC-4.0`, new events reported on GWOSC matched new events documented in each publication. For `GWTC-4.0` (Abac et al. 2025d), `GWTC-4.1`, and `GWTC-5.0` (Abac et al. 2026c), the events found in the Event Portal satisfy

$$p_{\rm astro} > 0.5 \text{ or } \mathrm{FAR} < 1\,\mathrm{yr}^{-1}, \tag{3}$$

[10] See https://gwosc.org/O3/auxiliary/ for O3 and https://gwosc.org/O4/auxiliary/ for O4a and O4b.

[11] GWOSC Event Portal, https://gwosc.org/eventapi

[12] GWOSC Client API, https://pypi.org/project/gwosc/

which may or may not agree completely with results tabulated in the publications. Here $p_{\rm astro}$ is the probability that a GW candidate is of astrophysical origin (Abac et al. 2026a).

`GWTC-4.1` results supersede those in `GWTC-4.0` and are identified as `GWTC-4.1`. However, as `GWTC` is a cumulative catalog, all the results labeled `GWTC-4.1` are included in the `GWTC-5.0` catalog by definition (Abac et al. 2026c).

Detailed documentation and references to publications are available for each release on the GWOSC website.

By selecting one of the releases, an *Event List* table is generated showing all events in the release, along with source parameters and credible intervals where available. The Event List view includes estimates of a number of physical parameters, such as mass, distance, and spin, as well as search-pipeline outputs such as SNR and FAR. If more than one parameter-estimation analysis is available for any event, then values from the analysis marked as `Default PE` for the specific event are displayed in the Event List to indicate which of the multiple results are captured in the table. Additionally, the lowest FAR and highest probability of astrophysical origin $p_{\rm astro}$ from all available search results are included in the Event List table.

A special case of the Event List view is the `GWTC` release, which always corresponds to an electronic version of the latest cumulative GWTC (currently GWTC-5.0; Abac et al. 2026a,b,c). Selecting the GWTC release returns this set of events as an Event List. It includes confidently detected events from multiple data releases.

Event Lists are also available to browse specific events using customized queries. Event Lists may include more than one version of an event, as some events have appeared in multiple publications, or have been re-analyzed with newer code or models. The *Query Page* presents the user with a form that allows selection of events based on name, membership in particular releases, various ranges of masses, distance, redshift, effective inspiral spin ($\chi_{\rm eff}$), $p_{\rm astro}$, SNR, FAR, UTC and GPS times. The query also allows specification of the output format to return, with support for `HTML`, `JSON`, `CSV` and `ASCII`.

The *Single Event View* shows key parameters for an individual event in the Event Portal. The view can include sets of parameters from different pipelines, including search-pipeline outputs such as SNR and FAR, and inferred source properties such as masses and spins. The Single Event View also includes images showing a spectrogram (Chatterji 2005) of the strain data for each detector at the time of the event, and links to download the associated strain time series in multiple file formats, as described in Section 5. The Single Event View also provides links to documentation, low-latency information in the Gravitational-Wave Candidate Event Database (GraceDB),[13] General Coordinates Network (GCN) Circulars and Notices, and links to segment lists for times around the event (see Section 5.2 for details). A new feature found on these pages is the Event Viewer which leads to a web app that generates plots of waveforms, source parameters and sky localization for each GW event.[14]

7.2. *Parameter-Estimation Results*

Most events in the Event Portal include one or more sets of credible intervals drawn from the publication associated with the event. The naming of parameters is based on the LVK standard names convention.[15] Many entries include multiple sets of values attributed to different priors, waveforms, or analysis changes (Abac et al. 2026b). In some cases, a publication will present credible intervals describing samples combined from several analyses using different waveform models. The results for any individual parameter are expressed as the median value with its 90% symmetric credible interval. Details regarding how the posterior samples were constructed can be found in the publication from which the event is released or in the supplemental releases linked from the Single Event View.

7.3. *Supplemental Data Releases*

For most events, the Single Event View includes links to supplemental data. These data vary between releases, but in general will include links to the parameter-estimation posterior samples, source localization, and additional resources. Supplemental data releases are published either in the LIGO Document Control Center[16] or under the LVK Zenodo Community.[17] In addition, GWOSC maintains snapshots of the Event Portal's version history as a data set available on Zenodo.[18] Each snapshot consists of `JSON` files downloaded from the Event Portal with data for each event.

7.4. *Community Catalogs*

The Event Portal has recently been extended to provide GW events from catalog authors outside of the LVK, which are collectively organized as *Community Catalogs*. The presentation of results for Community Catalogs is identical to that available with any LVK release of events, adhering to the website layout and search capabilities discussed previously. This is achieved by standardizing on a `JSON` schema file format for GWOSC staff to use to ingest search and parameter-estimation values. The details for this standard `JSON` are publicly available in GitHub,[19] along with useful test scripts, notebooks, and documentation. The criteria for authors outside the LVK Collaboration to have their

[13] GraceDB website, https://gracedb.ligo.org/

[14] GW Event Viewer, https://peviewer.igwn.org

[15] Parameter Estimation Name Standard, https://lscsoft.docs.ligo.org/pesummary/stable/gw/parameters.html

[16] Public LIGO Document Control Center, https://dcc.ligo.org/public/

[17] LVK Zenodo Data Releases, https://zenodo.org/communities/ligo-virgo-kagra/

[18] GWOSC Zenodo Event Portal Snapshots, http://doi.org/10.1088/1361-6382/ad0b9b

[19] GWOSC Github Community Catalog Schema, https://github.com/gwosc-tutorial/gwosc-catalog

Table 12. List of releases currently available under the GWOSC Event Portal.[a]

Release Name	Notes
GWTC	Cumulative set of GW transients maintained by the LVK (Abac et al. 2026a)
Initial_LIGO_Virgo	Event release from initial LIGO and Virgo, 2005–2010 (Abadie et al. 2012)
O1_O2-Preliminary	Notable events in O1 and O2 published prior to GWTC-1.0 release (Abbott et al. 2019)
GWTC-1-confident	Confident detections from the O1 and O2 runs (Abbott et al. 2019)
GWTC-1-marginal	Marginal candidates from O1 and O2 runs (Abbott et al. 2019)
GWTC-2	Confident detections from the O3a run (Abbott et al. 2021b)
GWTC-2.1-confident	Confident detections from O3a run based on a revised analysis (Abbott et al. 2024)
GWTC-2.1-marginal	Marginal candidates from O3a run based on a revised analysis (Abbott et al. 2024)
GWTC-2.1-auxiliary	Candidates from GWTC-2.0 that were demoted in GWTC-2.1 (Abbott et al. 2021b)
GWTC-3-confident	Confident detection from O3b run (Abbott et al. 2023b)
GWTC-3-marginal	Marginal candidates from O3b run (Abbott et al. 2023b)
IAS-O3a	Events from O3a as described in a community catalog (Olsen et al. 2022)
O3_Discovery_Papers	Notable events in O3 run published independently (Abbott et al. 2020c,d,e,f, 2021c)
O3_IMBH_marginal	Marginal intermediate-mass black hole candidates from O3 run Abbott et al. (2022)
O4_Discovery_Papers	Notable events in O4 run published independently (Abac et al. 2024, 2025a,e,f,g, 2026)
GWTC-4.0	Data release for O4a events (Abac et al. 2025d)
GWTC-4.1	Updated data release for O4a based on a revised analysis (Abac et al. 2026c)
GWTC-5.0	Data release for O4b events (Abac et al. 2026c)

[a] GWOSC Event Portal, https://gwosc.org/eventapi/html

catalogs included in GWOSC is documented in the *GWOSC Community Catalogs Guidelines*.[20]

8. SUMMARY

Data from the LVK network of observatories are publicly available through the GWOSC website at gwosc.org, and the latest update includes O4b data from LIGO and Virgo. This paper can serve as a practical guide for users interested in analyzing this set of open data. It provides important details about calibration and data quality, explains the structure of the data sets available online, and offers instructions for using the Event Portal, which gives access to the list of astrophysical sources identified by the LVK.

Making these resources available maximizes the scientific potential of the data set. The O4b data contain a wealth of compact object mergers, many of which are listed in version 5.0 of the Gravitational-Wave Transient Catalog (Abac et al. 2026c). By releasing the data publicly, the community is empowered to further explore and discover new insights.

The present release covers the second part of O4. The third part is planned for release in December 2026 (LIGO Laboratory 2025). With the completion of the O4 data set, we anticipate even more opportunities for discovery.

ACKNOWLEDGEMENTS

This material is based upon work supported by NSF's LIGO Laboratory, which is a major facility fully funded by the National Science Foundation. The authors also gratefully acknowledge the support of the Science and Technology Facilities Council (STFC) of the United Kingdom, the Max-Planck-Society (MPS), and the State of Niedersachsen/Germany for support of the construction of Advanced LIGO and construction and operation of the GEO 600 detector. Additional support for Advanced LIGO was provided by the Australian Research Council. The authors gratefully acknowledge the Italian Istituto Nazionale di Fisica Nucleare (INFN), the French Centre National de la Recherche Scientifique (CNRS) and the Netherlands Organization for Scientific Research (NWO) for the construction and operation of the Virgo detector and the creation and support of the EGO consortium. The authors also gratefully acknowledge research support from these agencies as well as by the Council of Scientific and Industrial Research of India, the Department of Science and Technology, India, the Science & Engineering Research Board (SERB), India, the Ministry of Human Resource Development, India, the Spanish Agencia Estatal de Investigación (AEI), the Spanish Ministerio de Ciencia, Innovación y Universidades, the European Union NextGenerationEU/PRTR (PRTR-C17.I1), the ICSC - CentroNazionale di Ricerca in High Performance Computing, Big Data and Quantum Computing, funded by the European Union NextGenerationEU, the Comunitat Autonòma de les Illes Balears through the Conselleria d'Educació i Universitats, the Conselleria d'Innovació,

[20] GWOSC Community Catalogs Guidelines, https://dcc.ligo.org/LIGO-M2500012/public

Universitats, Ciència i Societat Digital de la Generalitat Valenciana and the CERCA Programme Generalitat de Catalunya, Spain, the Polish National Agency for Academic Exchange, the National Science Centre of Poland and the European Union - European Regional Development Fund; the Foundation for Polish Science (FNP), the Polish Ministry of Science and Higher Education, the Swiss National Science Foundation (SNSF), the Russian Science Foundation, the European Commission, the European Social Funds (ESF), the European Regional Development Funds (ERDF), the Royal Society, the Scottish Funding Council, the Scottish Universities Physics Alliance, the Hungarian Scientific Research Fund (OTKA), the French Lyon Institute of Origins (LIO), the Belgian Fonds de la Recherche Scientifique (FRS-FNRS), Actions de Recherche Concertées (ARC) and Fonds Wetenschappelijk Onderzoek - Vlaanderen (FWO), Belgium, the Paris Île-de-France Region, the National Research, Development and Innovation Office of Hungary (NKFIH), the National Research Foundation of Korea, the Natural Sciences and Engineering Research Council of Canada (NSERC), the Canadian Foundation for Innovation (CFI), the Brazilian Ministry of Science, Technology, and Innovations, the International Center for Theoretical Physics South American Institute for Fundamental Research (ICTP-SAIFR), the Research Grants Council of Hong Kong, the National Natural Science Foundation of China (NSFC), the Israel Science Foundation (ISF), the US-Israel Binational Science Fund (BSF), the Leverhulme Trust, the Research Corporation, the National Science and Technology Council (NSTC), Taiwan, the United States Department of Energy, and the Kavli Foundation. The authors gratefully acknowledge the support of the NSF, STFC, INFN and CNRS for provision of computational resources.

This work was supported by MEXT, the JSPS Leading-edge Research Infrastructure Program, JSPS Grant-in-Aid for Specially Promoted Research 26000005, JSPS Grant-in-Aid for Scientific Research on Innovative Areas 2402: 24103006, 24103005, and 2905: JP17H06358, JP17H06361 and JP17H06364, JSPS Core-to-Core Program A. Advanced Research Networks, JSPS Grants-in-Aid for Scientific Research (S) 17H06133 and 20H05639, JSPS Grant-in-Aid for Transformative Research Areas (A) 20A203: JP20H05854, the joint research program of the Institute for Cosmic Ray Research, University of Tokyo, the National Research Foundation (NRF), the Computing Infrastructure Project of the Global Science experimental Data hub Center (GSDC) at KISTI, the Korea Astronomy and Space Science Institute (KASI), the Ministry of Science and ICT (MSIT) in Korea, Academia Sinica (AS), the AS Grid Center (ASGC) and the National Science and Technology Council (NSTC) in Taiwan under grants including the Science Vanguard Research Program, the Advanced Technology Center (ATC) of NAOJ, the Mechanical Engineering Center of KEK and Vietnam National Foundation for Science and Technology Development (NAFOSTED) 103.01-2025.147.

Additional acknowledgements for support of individual authors may be found in the following document: `https://dcc.ligo.org/LIGO-M2300033/public`.

Software: This software infrastructure used to publish data products onto the GWOSC website made significant use of the IGWN Software Environment (IGWN Computing and Software Working Group 2025) curated by the LVK to provide a reproducible computing environment built around tools needed for GW data analysis. Plots were prepared with `Matplotlib` (Hunter 2007).

DATA AVAILABILITY

All data products described in this work are publicly available on the Gravitational Wave Open Science Center,[21] the Zenodo LVK community page,[22] and through the OSDF and NDS2 data repositories, as described in the previous sections of this paper. Data products are provided under a Creative Commons Attribution 4.0 International license.[23]

APPENDIX

A. ADDITIONAL SEGMENTS IN THE O4A STRAIN-DATA RELEASE

The O4a run started on 24 May 2023 at 15:00 UTC. However, a few segments of data from the engineering run just prior to the start of the run were used in the search for GW emitted from SN 2023ixf (Abac et al. 2025h) and for the neutron star–black hole binary candidate GW230518_125908 (Abac et al. 2026c), and they have been added to this release. These additional data segments span between times 15 May 2023 14:13:22 UTC (GPS 1368195220) and 19 May 2023 17:31:33 UTC (GPS 1368552711) when both LHO and LLO were in observing mode. These segments have a total duration of 0.8 days. Including this addition, the total amount of observing time in O4a is 160.8 days for LHO and 164.3 days for LLO (to compare with Table 2, 0.8 days have to be added to the coincident times).

[21] GWOSC Home Page: https://gwosc.org

[22] Zenodo LVK Community Page: https://zenodo.org/communities/ligo-virgo-kagra/

[23] CC BY 4.0 license: https://creativecommons.org/licenses/by/4.0/

Using this total amount of time as reference, the percentage of the observing time for which the data quality pass each category described in Table 7 in O4a can be calculated. Since these percentages are close to 100%, Table 13 summarizes the percentages of failing times.

Table 13. Percentage of the observing time in O4a, including the extra 0.8 days of engineering run data, for which data quality fail the categories described in Table 7.

Short name	Percentage in LHO	Percentage in LLO
DATA	0.0971%	0.0059%
CBC_CAT1	0.0971%	0.0059%
CBC_CAT2	0.0971%	0.0059%
CBC_CAT3	0.0971%	0.0059%
BURST_CAT1	0.0971%	0.0059%
BURST_CAT2	0.2242%	0.1188%
BURST_CAT3	0.2242%	0.1188%
STOCH_CAT1	0.0979%	0.0065%
CW_CAT1	0.0971%	0.0059%

REFERENCES

Aasi, J., Abbott, B. P., Abbott, R., et al. 2015, Classical and Quantum Gravity, 32, 074001, doi: 10.1088/0264-9381/32/7/074001

Abac, A. G., Abouelfettouh, I., Acernese, F., et al. 2025a, arXiv e-prints, arXiv:2509.07348, doi: 10.48550/arXiv.2509.07348

Abac, A. G., Abouelfettouh, I., Acernese, F., et al. 2026a, To be published in this issue. https://dcc.ligo.org/LIGO-P2500701/public

—. 2026b, To be published in this issue. https://dcc.ligo.org/LIGO-P2600166/public

—. 2026c, To be published in this issue. https://dcc.ligo.org/LIGO-P2600152/public

Abac, A. G., Abbott, R., Abouelfettouh, I., et al. 2024, ApJL, 970, L34, doi: 10.3847/2041-8213/ad5beb

Abac, A. G., Abouelfettouh, I., Acernese, F., et al. 2025b, arXiv e-prints, arXiv:2508.18079, doi: 10.48550/arXiv.2508.18079

—. 2025c, ApJL, 995, L18, doi: 10.3847/2041-8213/ae0c06

—. 2025d, arXiv e-prints, arXiv:2508.18082, doi: 10.48550/arXiv.2508.18082

—. 2025e, ApJL, 993, L25, doi: 10.3847/2041-8213/ae0c9c

—. 2025f, ApJL, 993, L21, doi: 10.3847/2041-8213/ae0d54

—. 2025g, PhRvL, 135, 111403, doi: 10.1103/kw5g-d732

Abac, A. G., Abbott, R., Abouelfettouh, I., et al. 2025h, Astrophysical Journal, 985, 183, doi: 10.3847/1538-4357/adc681

Abac, A. G., Abouelfettouh, I., Acernese, F., et al. 2026, arXiv e-prints, arXiv:2605.11703. https://arxiv.org/abs/2605.11703

Abadie, J., Abbott, B. P., Abbott, R., et al. 2012, PhRvD, 85, 082002, doi: 10.1103/PhysRevD.85.082002

Abbott, B. P., Abbott, R., Adhikari, R., et al. 2009, Reports on Progress in Physics, 72, 076901, doi: 10.1088/0034-4885/72/7/076901

Abbott, B. P., Abbott, R., Abbott, T. D., et al. 2016, Classical and Quantum Gravity, 33, 134001, doi: 10.1088/0264-9381/33/13/134001

—. 2017, PhRvD, 95, 062003, doi: 10.1103/PhysRevD.95.062003

—. 2018, Classical and Quantum Gravity, 35, 065010, doi: 10.1088/1361-6382/aaaafa

—. 2019, Physical Review X, 9, 031040, doi: 10.1103/PhysRevX.9.031040

—. 2020a, Living Reviews in Relativity, 23, 3, doi: 10.1007/s41114-020-00026-9

—. 2020b, Classical and Quantum Gravity, 37, 055002, doi: 10.1088/1361-6382/ab685e

—. 2020c, ApJL, 892, L3, doi: 10.3847/2041-8213/ab75f5

Abbott, R., Abbott, T. D., Abraham, S., et al. 2020d, PhRvD, 102, 043015, doi: 10.1103/PhysRevD.102.043015

—. 2020e, ApJL, 900, L13, doi: 10.3847/2041-8213/aba493

—. 2020f, ApJL, 896, L44, doi: 10.3847/2041-8213/ab960f

—. 2021a, SoftwareX, 13, 100658, doi: 10.1016/j.softx.2021.100658

—. 2021b, Physical Review X, 11, 021053, doi: 10.1103/PhysRevX.11.021053

—. 2021c, ApJL, 915, L5, doi: 10.3847/2041-8213/ac082e

Abbott, R., Abe, H., Acernese, F., et al. 2022, Progress of Theoretical and Experimental Physics, 2022, 063F01, doi: 10.1093/ptep/ptac073

Abbott, R., Abbott, T. D., Acernese, F., et al. 2022, A&A, 659, A84, doi: 10.1051/0004-6361/202141452

Abbott, R., Abe, H., Acernese, F., et al. 2023a, ApJS, 267, 29, doi: 10.3847/1538-4365/acdc9f

Abbott, R., Abbott, T. D., Acernese, F., et al. 2023b, Physical Review X, 13, 041039, doi: 10.1103/PhysRevX.13.041039

—. 2024, PhRvD, 109, 022001, doi: 10.1103/PhysRevD.109.022001

Acernese, F., Agapito, A., Agarwal, D., et al. 2026, Calibration of Advanced Virgo and reconstruction of the detector strain h(t) in O4

Acernese, F., Agathos, M., Agatsuma, K., et al. 2015, Classical and Quantum Gravity, 32, 024001, doi: 10.1088/0264-9381/32/2/024001

Acernese, F., Adams, T., Agatsuma, K., et al. 2018, Classical and Quantum Gravity, 35, 205004, doi: 10.1088/1361-6382/aadf1a

Acernese, F., Agathos, M., Ain, A., et al. 2022, Classical and Quantum Gravity, 39, 045006, doi: 10.1088/1361-6382/ac3c8e

—. 2023, Classical and Quantum Gravity, 40, 185006, doi: 10.1088/1361-6382/acd92d

Acernese, F., Agathos, M., Ain, A., et al. 2023, Classical and Quantum Gravity, 40, 185005, doi: 10.1088/1361-6382/acdf36

Affeldt, C., Danzmann, K., Dooley, K. L., et al. 2014, Classical and Quantum Gravity, 31, 224002, doi: 10.1088/0264-9381/31/22/224002

Akutsu, T., Ando, M., Arai, K., et al. 2021a, Progress of Theoretical and Experimental Physics, 2021, 05A101, doi: 10.1093/ptep/ptaa125

—. 2021b, Progress of Theoretical and Experimental Physics, 2021, 05A102, doi: 10.1093/ptep/ptab018

Allen, B. 1997, Les Houches school of physics: astrophysical sources of gravitational radiation, 373

Alléné, C., Aubin, F., Bentara, I., et al. 2025, Classical and Quantum Gravity, 42, 105009, doi: 10.1088/1361-6382/add234

Aubin, F., Dangelser, E., Estevez, D., et al. 2024, Classical and Quantum Gravity, 41, 235003, doi: 10.1088/1361-6382/ad869c

Bhattacharjee, D., Savage, R. L., Bajpai, R., et al. 2024, Metrologia, 61, 054002, doi: 10.1088/1681-7575/ad615f

Biwer, C., Barker, D., Batch, J. C., et al. 2017, Physical Review D, 95, 062002, doi: 10.1103/PhysRevD.95.062002

Brooks, A. F., Vajente, G., Yamamoto, H., et al. 2021, ApOpt, 60, 4047, doi: 10.1364/AO.419689

Buikema, A., Cahillane, C., Mansell, G. L., et al. 2020, PhRvD, 102, 062003, doi: 10.1103/PhysRevD.102.062003

Cahillane, C., Betzwieser, J., Brown, D. A., et al. 2017, PhRvD, 96, 102001, doi: 10.1103/PhysRevD.96.102001

Capote, E., Jia, W., Aritomi, N., et al. 2025, PhRvD, 111, 062002, doi: 10.1103/PhysRevD.111.062002

Caudill, S., Kandhasamy, S., Lazzaro, C., et al. 2021, Mod. Phys. Lett. A, 36, 2130022, doi: 10.1142/S0217732321300226

Chandra, K., Villa-Ortega, V., Dent, T., et al. 2021, PhRvD, 104, 042004, doi: 10.1103/PhysRevD.104.042004

Chatterji, S. K. 2005, PhD thesis, Massachusetts Institute of Technology

Chen, D., Hido, S., Tuyenbayev, D., et al. 2025, arXiv e-prints, arXiv:2504.12657, doi: 10.48550/arXiv.2504.12657

Chen, H.-Y., Holz, D. E., Miller, J., et al. 2021, Classical and Quantum Gravity, 38, 055010, doi: 10.1088/1361-6382/abd594

Cornish, N. J., Littenberg, T. B., Bécsy, B., et al. 2021, PhRvD, 103, 044006, doi: 10.1103/PhysRevD.103.044006

Covas, P. B., Effler, A., Goetz, E., et al. 2018, PhRvD, 97, 082002, doi: 10.1103/PhysRevD.97.082002

Davis, D., Massinger, T., Lundgren, A., et al. 2019, Classical and Quantum Gravity, 36, 055011, doi: 10.1088/1361-6382/ab01c5

Davis, D., Neunzert, A., Goetz, E., et al. 2024, Self-gating of O4a h(t) for use in continuous-wave searches, Tech. Rep. LIGO-T2400003. https://dcc.ligo.org/LIGO-T2400003/public

Davis, D., Areeda, J. S., Berger, B. K., et al. 2021, Classical and Quantum Gravity, 38, 135014, doi: 10.1088/1361-6382/abfd85

Di Renzo, F. 2023, Virgo Logbook, 59763

Dooley, K. L., Leong, J. R., Adams, T., et al. 2016, Classical and Quantum Gravity, 33, 075009, doi: 10.1088/0264-9381/33/7/075009

Driggers, J. C., Vitale, S., Lundgren, A. P., et al. 2019, PhRvD, 99, 042001, doi: 10.1103/PhysRevD.99.042001

Ertini, K., Regna, T. A., Ferrari, L., et al. 2025, A&A, 699, A60, doi: 10.1051/0004-6361/202554333

Essick, R., Godwin, P., Hanna, C., Blackburn, L., & Katsavounidis, E. 2020, Machine Learning: Science and Technology, 2, 015004, doi: 10.1088/2632-2153/abab5f

Essick, R., Mo, G., & Katsavounidis, E. 2021, PhRvD, 103, 042003, doi: 10.1103/PhysRevD.103.042003

Estevez, D., Lagabbe, P., Masserot, A., et al. 2021a, Classical and Quantum Gravity, 38, 075007. https://arxiv.org/abs/2009.08103

Estevez, D., Mours, B., & Pradier, T. 2021b, Classical and Quantum Gravity, 38, 075012, doi: 10.1088/1361-6382/abe2da

Finn, L. S., & Chernoff, D. F. 1993, PhRvD, 47, 2198, doi: 10.1103/PhysRevD.47.2198

Ghonge, S., Brandt, J., Sullivan, J. M., et al. 2024, Phys. Rev. D, 110, 122002, doi: 10.1103/PhysRevD.110.122002

Glanzer, J., Banagiri, S., Coughlin, S. B., et al. 2023, Classical and Quantum Gravity, 40, 065004, doi: 10.1088/1361-6382/acb633

Godwin, P., Essick, R., Hanna, C., et al. 2020, arXiv e-prints, arXiv:2010.15282, doi: 10.48550/arXiv.2010.15282

Goetz, E., Neunzert, A., Knee, A., et al. 2026, O4ab lines and combs in found in self-gated C00 cleaned data, Tech. Rep. LIGO-T2500212, LIGO Laboratory. https://dcc.ligo.org/T2500212/public

Grimaud, C. 2025, Phd thesis, Université Savoie Mont Blanc

Grimaud, C., et al. 2026, Journal of Physics: Conference Series, 3177, 012082, doi: https://doi.org/10.1088/1742-6596/3177/1/012082

Gurav, R., Kelly, I., Goodarzi, P., et al. 2024, doi: 10.1109/BigData62323.2024.10825388

Hourihane, S., Chatziioannou, K., Wijngaarden, M., et al. 2022, PhRvD, 106, 042006, doi: 10.1103/PhysRevD.106.042006

Hunter, J. D. 2007, Computing in Science and Engineering, 9, 90, doi: 10.1109/MCSE.2007.55

Huxford, R., George, R., Trevor, M., Yarbrough, Z., & Godwin, P. 2024, arXiv e-prints, arXiv:2412.04638, doi: 10.48550/arXiv.2412.04638

IGWN Computing and Software Working Group. 2025, IGWN Conda Environment, https://computing.docs.ligo.org/conda/

Jia, W., Xu, V., Kuns, K., et al. 2024, Science, 385, 1318, doi: 10.1126/science.ado8069

Karki, S., Tuyenbayev, D., Kandhasamy, S., et al. 2016, Review of Scientific Instruments, 87, 114503, doi: 10.1063/1.4967303

Koziol, Q., & Robinson, D. 2018, HDF5. https://doi.org/10.11578/dc.20180330.1

Kwok, J. Y. L., Lo, R. K. L., Weinstein, A. J., & Li, T. G. F. 2022, PhRvD, 105, 024066, doi: 10.1103/PhysRevD.105.024066

Lecoeuche, Y., McIver, J., Knee, A. M., et al. 2026, arXiv preprint arXiv:2604.07668

LIGO–Virgo. 2022, Specification of a Common Data Frame Format for Interferometric Gravitational Wave Detectors (v4), Tech. Rep. VIR-067A-08. https://dcc.ligo.org/LIGO-T970130/public

LIGO–Virgo–KAGRA. 2017, Data release for event GW170817, doi: 10.7935/K5B8566F

—. 2019. https://dcc.ligo.org/LIGO-M1900145/public

—. 2021a. https://dcc.ligo.org/T2100313/public

—. 2021b, O3a Data Release, doi: 10.7935/nfnt-hm34

—. 2021c, O3b Data Release, doi: 10.7935/pr1e-j706

—. 2022, O3GK Data Release, doi: 10.7935/38s2-7g84

—. 2024, GEO600 Data for FRBs from SGR 1935+2154, doi: 10.7935/j4zw-0376

—. 2025a. https://dcc.ligo.org/T2500288/public

—. 2025b. https://doi.org/10.5281/zenodo.16856919

—. 2025c, O4a Data Release, doi: 10.7935/kt51-6n86

—. 2026, O4b Data Release, doi: TODO

LIGO Laboratory. 2025. https://dcc.ligo.org/LIGO-M1000066/public

Lück, H., Affeldt, C., Degallaix, J., et al. 2010, in Journal of Physics Conference Series, Vol. 228, Journal of Physics Conference Series (IOP), 012012, doi: 10.1088/1742-6596/228/1/012012

Macas, R., Pooley, J., Nuttall, L. K., et al. 2022, PhRvD, 105, 103021, doi: 10.1103/PhysRevD.105.103021

Macleod, D. M., Areeda, J. S., Coughlin, S. B., Massinger, T. J., & Urban, A. L. 2021, SoftwareX, 13, 100657, doi: 10.1016/j.softx.2021.100657

Nguyen, P., Schofield, R. M. S., Effler, A., et al. 2021, Classical and Quantum Gravity, 38, 145001, doi: 10.1088/1361-6382/ac011a

Nuttall, L. K. 2018, Philosophical Transactions of the Royal Society of London Series A, 376, 20170286, doi: 10.1098/rsta.2017.0286

Nuttall, L. K., Massinger, T. J., Areeda, J., et al. 2015, Classical and Quantum Gravity, 32, 245005, doi: 10.1088/0264-9381/32/24/245005

Nyquist, H. 1924, Bell System Technical Journal, 3, 324, doi: 10.1002/j.1538-7305.1924.tb01361.x

Olsen, S., Venumadhav, T., Mushkin, J., et al. 2022, PhRvD, 106, 043009, doi: 10.1103/PhysRevD.106.043009

Pankow, C., Chatziioannou, K., Chase, E. A., et al. 2018, PhRvD, 98, 084016, doi: 10.1103/PhysRevD.98.084016

Powell, J., & Lasky, P. D. 2025, The DAWES review: Gravitational-wave burst astrophysics. https://arxiv.org/abs/2410.12105

Riles, K. 2023, Living Reviews in Relativity, 26, 3, doi: 10.1007/s41114-023-00044-3

Rolland, L., & Verkindt, D. 2025. https://tds.virgo-gw.eu/ql/?c=22019

Rollins, J. G. 2016, Review of Scientific Instruments, 87, 094502, doi: 10.1063/1.4961665

Romano, J. D., & Cornish, N. J. 2017, Living Reviews in Relativity, 20, 2, doi: 10.1007/s41114-017-0004-1

Smith, S. W. 1999, The Scientist and Engineer's Guide to Digital Signal Processing (California Technical Publishing). www.DSPguide.com

Soni, S., Glanzer, J., Effler, A., et al. 2024, Class. Quant. Grav., 41, 135015, doi: 10.1088/1361-6382/ad494a

Soni, S., Austin, C., Effler, A., et al. 2021, Classical and Quantum Gravity, 38, 025016, doi: 10.1088/1361-6382/abc906

Soni, S., Berger, B. K., Davis, D., et al. 2025, Classical and Quantum Gravity, 42, 085016, doi: 10.1088/1361-6382/adc4b6

Sun, L., Goetz, E., Kissel, J. S., et al. 2020, Classical and Quantum Gravity, 37, 225008, doi: 10.1088/1361-6382/abb14e

—. 2021, arXiv e-prints, arXiv:2107.00129, doi: 10.48550/arXiv.2107.00129

Syx, A. 2025, Phd thesis, Université de Strasbourg

Tse, M., Yu, H., Kijbunchoo, N., et al. 2019, PhRvL, 123, 231107, doi: 10.1103/PhysRevLett.123.231107

Usman, S. A., Nitz, A. H., Harry, I. W., et al. 2016, Classical and Quantum Gravity, 33, 215004, doi: 10.1088/0264-9381/33/21/215004

Vajente, G., Huang, Y., Isi, M., et al. 2020, PhRvD, 101, 042003, doi: 10.1103/PhysRevD.101.042003

Vallisneri, M., Kanner, J., Williams, R., Weinstein, A., & Stephens, B. 2015, Journal of Physics Conference Series, 610, 012021, doi: 10.1088/1742-6596/610/1/012021

Verkindt, D., et al. 2026, Journal of Physics: Conference Series, 3177, 012068, doi: https://doi.org/10.1088/1742-6596/3177/1/012068

Viets, A., & Wade, M. 2021. https://dcc.ligo.org/LIGO-T2100058/public

Viets, A. D. 2019, PhD thesis, University of Wisconsin-Milwaukee. https://wisconsin.edu

Viets, A. D., Wade, M., Urban, A. L., et al. 2018, Classical and Quantum Gravity, 35, 095015, doi: 10.1088/1361-6382/aab658

Virtanen, P., Gommers, R., Oliphant, T. E., et al. 2020, Nature Medicine, 17, 261, doi: 10.1038/s41592-019-0686-2

Wade, M., et al. 2025. https://arxiv.org/abs/2508.08423

Zackay, B., Venumadhav, T., & Zaldarriaga, M. 2023, Application for the release of a set of auxiliary channels from the O3, Tech. Rep. T2300274. https://dcc.ligo.org/LIGO-T2300274/public

Zweizig, J., Maros, E., Hanks, J., & Areeda, J. 2021. https://wiki.ligo.org/Computing/NDSClient/

Zweizig, J., & Riles, K. 2020, Information on self-gating of $h(t)$ used in O3 continuous-wave and stochastic searches, Tech. Rep. T2000384. https://dcc.ligo.org/LIGO-T2000384/public